

Is It Possible to Study the Wave Function of $2S$ Vector Mesons at HERA ?

Jan Nemchik

*Institute of Experimental Physics SAS,
Watsonova 47,
04353 Kosice,
Slovakia*

Abstract

We present a short review of anomalous properties in diffractive photo- and electroproduction of radially excited $V'(2S)$ vector mesons. Using the color dipole gBFKL phenomenology we analyze anomalous Q^2 and energy dependence of the production cross section, $V'(2S)/V(1S)$ production ratio, the diffraction slope and anomalous t behaviour of the differential cross section $d\sigma/dt$. The origin of these anomalies is based on the interplay of the nodal structure of $V'(2S)$ radial wave function with the energy and dipole size dependence of the dipole cross section and the diffraction slope. We analyze how a different pattern of anomalous behaviour of $V'(2S)$ production leads to a different position of the node in the wave function and discuss how that node position can be extracted from the data at HERA.

1 Introduction

The main goal of this paper is to present a short review of possible anomalies, which can be observed in diffractive photo- and electroproduction of radially excited $V'(2S)$ vector mesons

$$\gamma^* p \rightarrow V'(2S)p \quad V'(2S) = \rho', \Phi', \omega', \Psi', \Upsilon', \dots \quad (1)$$

Diffractive electroproduction of ground state $V(1S)$ vector mesons at high c.m.s. energy $W = \sqrt{s}$ is intensively discussed during the last decade and is very convenient for study of the pomeron exchange [1, 2, 3, 4, 5, 6, 7, 8, 9]. The standard approach to the pQCD is based on the BFKL equation [10, 11, 12] formulated in the scaling approximation of the infinite gluon correlation radius $R_c \rightarrow \infty$ (massless gluons) and of the fixed running coupling $\alpha_S = const.$ Later, however, a novel s -channel approach to the LLs BFKL equation (running gBFKL approach) has been developed [13, 14] in terms of the color dipole cross section $\sigma(\xi, r)$ (r is the transverse size of the color dipole, $\xi = \log(\frac{W^2+Q^2}{m_V^2+Q^2})$ is the rapidity variable) and incorporates consistently the asymptotic freedom (AF) (i.e. the running QCD coupling $\alpha_S(r)$) and the finite propagation radius R_c of perturbative gluons.

As a consequence of the gBFKL phenomenology for diffractive production of light [6, 15] and heavy [16] vector mesons is so-called *scanning phenomenon* [17, 4, 5, 6]; the $V(1S)$ vector meson production amplitude probes the color dipole cross section at the dipole size $r \sim r_S$, where the scanning radius r_S can be expressed through the scale parameter A

$$r_S \approx \frac{A}{\sqrt{m_V^2 + Q^2}}, \quad (2)$$

where Q^2 is the photon virtuality, m_V is the vector meson mass, $A \approx 6$ and slightly rises with Q^2 . Consequently, changing Q^2 and the mass of the produced vector meson one can probe the dipole cross section $\sigma(\xi, r)$ in a very broad range of the dipole sizes r . This fact allows to study the transition from large nonperturbative dipole size $r_S \gg R_c$ to the perturbative region of very short $r_S \ll R_c$. Furthermore, the scanning phenomenon give a possibility to study one important consequence of the color dipole gBFKL dynamics - the steeper subasymptotic energy dependence of the dipole cross section at smaller dipole sizes **r**.

Diffractive electroproduction of radially excited $V'(2S)$ vector mesons supplies us with an additional information on the dipole cross section. The presence of the node in $V'(2S)$ radial wave function leads to a strong cancellation of dipole size contributions to the production amplitude from the region above and below the node position r_n (the node effect [2, 17, 4, 18, 15, 16]). For this reason the amplitudes for electroproduction of the $V(1S)$ and $V'(2S)$ vector mesons probe $\sigma(\xi, r)$ in a different way.

The node effect as the dynamical mechanism has a lot of very interesting consequences in production of $V'(2S)$ vector mesons and can be tested at HERA. Therefore, we present a short review of different aspects and manifestations of the node effect. Firstly, we show the onset of a strong node effect in electroproduction of $V'(2S)$ light vector mesons [15], which leads to a very spectacular pattern of anomalous Q^2 and energy dependence of production cross section. More heavy is the vector meson much weaker is the node effect. However, for electroproduction of $V'(2S)$ heavy vector mesons much weaker node effect still leads to a slightly different Q^2 - and energy dependence of production cross section for Ψ' vs. J/Ψ and to a nonmonotonic Q^2 - dependence of the diffraction slope at small $Q^2 \lesssim 5 \text{ GeV}^2$ for Ψ' production [16]. Then we discuss another manifestation of the node effect experimentally confirmed at fixed target and HERA experiments in J/Ψ and Ψ' photoproduction; a strong

suppression of diffractive production of $V'(2S)$ vs. $V(1S)$ mesons. The stronger is the node effect the smaller is the $V'(2S)/V(1S)$ production ratio. The node effect in conjunction with the emerging gBFKL phenomenology of the diffraction slope [19, 20, 16] also leads to a counterintuitive inequality $B(\gamma^* \rightarrow \Psi') \lesssim B(\gamma^* \rightarrow J/\Psi)$ [16], which can be also tested at HERA. However, we show that above counterintuitive inequality $B(2S) < B(1S)$ is not always valid for $V'(2S)$ light vector meson production [22]. Finally, we analyze the node effect and its manifestation resulting in a very spectacular pattern of anomalous t dependence of the differential cross section [21]. In all the cases the main emphasize will be related to the production of $V'(2S)$ light vector mesons where the node effect is expected to be very strong. Also we find a correspondence between a specific pattern of anomalous behaviours and the position of the node in $V'(2S)$ radial wave function.

The paper is organized as follows. In Sect. 2 we present a very short review of the color dipole phenomenology of diffractive photo- and electroproduction of vector mesons. In Sect. 3 we analyze the anomalies in production cross section for $V'(2S)$ vector mesons. Sect. 4 is devoted to anomalous pattern of Q^2 and energy dependence of the diffraction slope for $V'(2S)$ production. In Sect. 5 we study anomalous t behaviour of the differential cross section $d\sigma(\gamma^* \rightarrow V'(2S))/dt$ at different Q^2 and energies. In all the cases we discuss how the position of the node in $V'(2S)$ radial wave function can be extracted from the data. The summary and conclusions are presented in Sect. 6.

2 Color dipole phenomenology for vector meson production. A short review.

The light-cone representation introduced in [23] represents very popular and powerful tool for study of the dynamics of vector meson diffractive photo- and electroproduction. The central point of this approach is that in the mixed (\mathbf{r}, z) representation the high energy vector meson can be treated as a system of color dipole described by the distribution of the transverse separation \mathbf{r} of the quark and antiquark given by the $q\bar{q}$ wave function, $\Psi(\mathbf{r}, z)$, where z is the fraction of meson's light-cone momentum carried by a quark. In this approach the imaginary part of the production amplitude for the real (virtual) photoproduction of vector mesons with the momentum transfer \mathbf{q} can be represented in the factorized form

$$\text{Im}\mathcal{M}(\gamma^* \rightarrow V, \xi, Q^2, \mathbf{q}) = \langle V | \sigma(\xi, r, z, \mathbf{q}) | \gamma^* \rangle = \int_0^1 dz \int d^2\mathbf{r} \sigma(\xi, r, z, \mathbf{q}) \Psi_V^*(\mathbf{r}, z) \Psi_{\gamma^*}(\mathbf{r}, z) \quad (3)$$

whose normalization is $d\sigma/dt|_{t=0} = |\mathcal{M}|^2/16\pi$. In Eq. (4), $\Psi_{\gamma^*}(\mathbf{r}, z)$ and $\Psi_V(\mathbf{r}, z)$ represent the probability amplitudes to find the color dipole of size r in the photon and quarkonium (vector meson), respectively. The color dipole distribution in (virtual) photons was derived in [24, 13]. $\sigma(\xi, r, z, \mathbf{q})$ in Eq (4) is the dipole scattering matrix for $q\bar{q} - N$ interaction. At $\mathbf{q} = 0$ it represents the color dipole cross section, which quantifies the interaction of the relativistic color dipole of the dipole size \mathbf{r} with the target nucleon. The dipole cross section $\sigma(\xi, r)$ is flavor independent and represents the universal function of r which describes various diffractive processes in unified form. Energy dependence of the dipole cross section reflexes an importance of the higher Fock states $q\bar{q}g\dots$ at high c.m.s. energy W . In the leading-log $\frac{1}{x}$ approximation the effect of higher Fock states can be reabsorbed into the energy dependence of $\sigma(\xi, r)$, which satisfies the gBFKL equation [13, 14] for the energy evolution.

At small \mathbf{q} considered in this paper, one can safely neglect the z -dependence of $\sigma(\xi, r, z, \mathbf{q})$ for light and heavy vector meson production and set $z = \frac{1}{2}$. This follows also from the analysis within double gluon exchange approximation [24] leading to a slow z dependence of the dipole cross section.

The detailed discussion about the space-time pattern of diffractive electroproduction of vector mesons is presented in [15, 16]. The energy dependence of the dipole cross section is quantified in terms of the dimensionless rapidity $\xi = \log \frac{1}{x_{eff}}$, x_{eff} is the effective value of the Bjorken variable

$$x_{eff} = \frac{Q^2 + m_V^2}{Q^2 + W^2} \approx \frac{m_V^2 + Q^2}{2\nu m_p}, \quad (4)$$

where m_p and m_V is the proton mass and mass of vector meson, respectively. Hereafter, we will write the energy dependence of the dipole cross section in both variables, either in ξ or in x_{eff} whenever convenient.

The production amplitudes for the transversely (T) and the longitudinally (L) polarized vector mesons with the small momentum transfer \mathbf{q} can be written in more explicit form [6, 16]

$$\begin{aligned} \text{Im}\mathcal{M}_T(x_{eff}, Q^2, \mathbf{q}) &= \frac{N_c C_V \sqrt{4\pi\alpha_{em}}}{(2\pi)^2} \cdot \\ &\cdot \int d^2\mathbf{r} \sigma(x_{eff}, r, \mathbf{q}) \int_0^1 \frac{dz}{z(1-z)} \left\{ m_q^2 K_0(\varepsilon r) \phi(r, z) - [z^2 + (1-z)^2] \varepsilon K_1(\varepsilon r) \partial_r \phi(r, z) \right\} \end{aligned} \quad (5)$$

$$\begin{aligned} \text{Im}\mathcal{M}_L(x_{eff}, Q^2, \mathbf{q}) &= \frac{N_c C_V \sqrt{4\pi\alpha_{em}} 2\sqrt{Q^2}}{(2\pi)^2 m_V} \cdot \\ &\cdot \int d^2\mathbf{r} \sigma(x_{eff}, r, \mathbf{q}) \int_0^1 dz \left\{ [m_q^2 + z(1-z)m_V^2] K_0(\varepsilon r) \phi(r, z) - \partial_r^2 \phi(r, z) \right\} \end{aligned} \quad (6)$$

where

$$\varepsilon^2 = m_q^2 + z(1-z)Q^2, \quad (7)$$

α_{em} is the fine structure constant, $N_c = 3$ is the number of colors, $C_V = \frac{1}{\sqrt{2}}, \frac{1}{3\sqrt{2}}, \frac{1}{3}, \frac{2}{3}, \frac{1}{3}$ for $\rho^0, \omega^0, \phi^0, J/\Psi, \Upsilon$ production, respectively and $K_{0,1}(x)$ are the modified Bessel functions. The discussion and parameterization of the light-cone radial wave function $\phi(r, z)$ of the $q\bar{q}$ Fock state of the vector meson is given in [15].

Following the scanning phenomenon (see Eq. (2)) one needs rather high values of $Q^2 \gtrsim 70 \text{ GeV}^2$ to reach the pure perturbative region $r \lesssim R_c$. Consequently, due to a very slow onset of the pure perturbative region one can easily anticipate a contribution to the production amplitude coming from the semiperturbative and nonperturbative $r \gtrsim R_c$. Following the simplest assumption about an additive property of the perturbative and nonperturbative mechanism of interaction we can represent the contribution of the bare pomeron exchange to $\sigma(\xi, r, \mathbf{q})$ as a sum of the perturbative and nonperturbative component ¹

$$\sigma(\xi, r, \mathbf{q}) = \sigma_{pt}(\xi, r, \mathbf{q}) + \sigma_{npt}(\xi, r, \mathbf{q}), \quad (8)$$

with the parameterization of both components at small \mathbf{q}

$$\sigma_{pt, npt}(\xi, r, \mathbf{q}) = \sigma_{pt, npt}(\xi, r, \mathbf{q} = 0) \exp\left(-\frac{1}{2} B_{pt, npt}(\xi, r) \mathbf{q}^2\right). \quad (9)$$

¹ additive property of such a decomposition of the dipole cross section has been already discussed in [15, 16]

Here $\sigma_{pt,npt}(\xi, r, \mathbf{q} = 0) = \sigma_{pt,npt}(\xi, r)$ represent the contribution of the perturbative and non-perturbative mechanism to the $q\bar{q}$ -nucleon interaction cross section, respectively, $B_{pt}(\xi, r)$ and $B_{npt}(\xi, r)$ are the corresponding dipole diffraction slopes.

The model predictions include also a small real part of production amplitudes taken in the form [25]

$$\text{Re}\mathcal{M}(\xi, r) = \frac{\pi}{2} \cdot \frac{\partial}{\partial \xi} \text{Im}\mathcal{M}(\xi, r). \quad (10)$$

The formalism for calculation of $\sigma_{pt}(\xi, r)$ in the leading-log s approximation was developed in [24, 13, 14]. The contribution $\sigma_{npt}(\xi, r)$ representing the soft nonperturbative component of the pomeron is a simple Regge pole with the intercept $\Delta_{npt} = 0$. The particular form together with assumption of the energy independent $\sigma_{npt}(\xi = \xi_0, r) = \sigma_{npt}(r)$ (ξ_0 corresponds to boundary condition for the gBFKL evolution, $\xi_0 = \log(1/x_0)$, $x_0 = 0.03$) allows us to successfully describe the proton structure function at very small Q^2 [26], the real photoabsorption [6] and diffractive real and virtual photoproduction of light [15] and heavy [16] vector mesons. Besides, the reasonable form of $\sigma_{npt}(r)$ was confirmed in the process of the first determination of the dipole cross section from the data on vector meson electroproduction [27] what is shown in Fig. 1. The energy and dipole size dependence of so-extracted $\sigma(\xi, r)$ is in a good agreement with the dipole cross section obtained from the gBFKL dynamics [6, 26]. The nonperturbative component of the pomeron exchange plays a dominant role at low NMC energies in the production of the light vector mesons. However, the perturbative component of the pomeron becomes more important with the rising energy also in the nonperturbative region of dipole sizes.

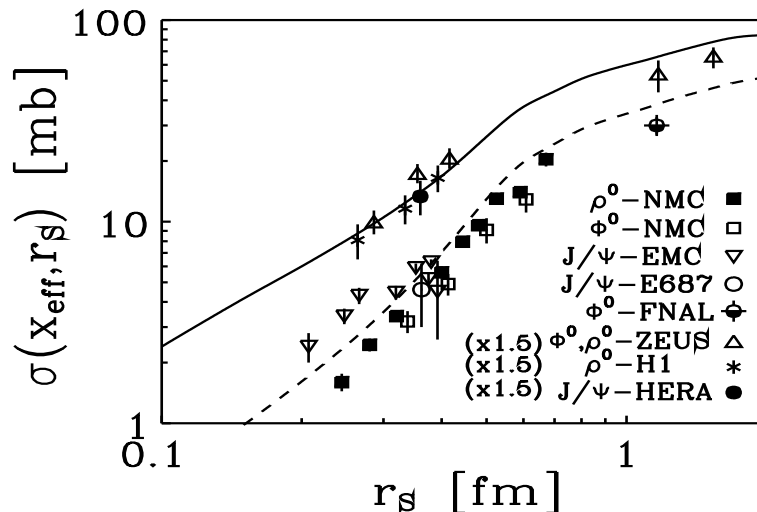


Figure 1: The dipole size dependence of the dipole cross section extracted from the data on photoproduction and electroproduction of vector mesons. The data are described in [6]. The dashed and solid curve show the dipole cross section of the model [26, 6] evaluated for the c.m.s. energy $W = 15$ and 70 GeV respectively. The data points at HERA energies and the corresponding solid curve are multiplied by the factor 1.5.

The generalization of the color dipole factorization formula (3) to the diffraction slope

of the reaction $\gamma^* p \rightarrow V p$ reads [16]

$$B(\gamma^* \rightarrow V, \xi, Q^2) \text{Im} \mathcal{M}(\gamma^* \rightarrow V, \xi, Q^2, \mathbf{q} = 0) = \int_0^1 dz \int d^2 \mathbf{r} \sigma(\xi, r) B(\xi, r) \Psi_V^*(r, z) \Psi_{\gamma^*}(r, z). \quad (11)$$

The diffraction cone in the color dipole gBFKL approach was studied in detail in [16]. Therefore, here we present only the salient feature of the color diffraction slope $B(\xi, r)$ emphasizing the presence of the geometrical contribution from beam dipole - $r^2/8$ and the contribution from the target proton size - $R_N^2/3$:

$$B(\xi, r) = \frac{1}{8} r^2 + \frac{1}{3} R_N^2 + 2\alpha'_{\mathbf{P}}(\xi - \xi_0) + \mathcal{O}(R_c^2), \quad (12)$$

where R_N is the radius of the proton. The term $2\alpha'_{\mathbf{P}}(\xi - \xi_0)$ describe the familiar Regge growth of $B(\xi, r)$ for the quark-quark scattering. The geometrical contribution to the diffraction slope from the target proton size $\frac{1}{3}R_N^2$ persists for all the dipole sizes $r \gtrsim R_c$ and $r \lesssim R_c$. The last term in (12) is also associated with the proton size and is negligibly small. The diffractive scattering of large color dipole has been also studied in the paper [16]. Here we assume the conventional Regge rise of the diffraction slope for the soft pomeron [16]

$$B_{npt}(\xi, r) = \Delta B_d(r) + \Delta B_N + 2\alpha'_{npt}(\xi - \xi_0), \quad (13)$$

where $\Delta B_d(r)$ and ΔB_N stand for the contribution from the beam dipole and target nucleon size. As a guidance the data on the pion-nucleon scattering [28] were used, which suggest $\alpha'_{npt} = 0.15 \text{ GeV}^{-2}$. In (13) the proton size contribution is

$$\Delta B_N = \frac{1}{3} R_N^2, \quad (14)$$

and the beam dipole contribution has been proposed to have a form [16]

$$\Delta B_d(r) = \frac{r^2}{8} \cdot \frac{r^2 + aR_N^2}{3r^2 + aR_N^2}, \quad (15)$$

where a is a phenomenological parameter, $a \sim 1$. We take $\Delta B_N = 4.8 \text{ GeV}^{-2}$. Then the pion-nucleon diffraction slope is reproduced with reasonable value of the parameter a in the formula (15): $a = 0.9$ for $\alpha'_{npt} = 0.15 \text{ GeV}^{-2}$.

Energy dependence of the gBFKL diffraction slope $B(\xi, r)$ (see Eq. (12) and [19]) can be evaluated through the energy dependent effective Regge slope $\alpha'_{eff}(\xi, r)$

$$B_{pt}(\xi, r) \approx \frac{1}{3} \langle R_N^2 \rangle + \frac{1}{8} r^2 + 2\alpha'_{eff}(\xi, r)(\xi - \xi_0). \quad (16)$$

The effective Regge slope $\alpha'_{eff}(\xi, r)$ varies with energy differently at different dipole size [19]. At fixed scanning radius and/or $Q^2 + m_V^2$, it decreases with energy. At fixed rapidity ξ and/or x_{eff} (4), $\alpha'_{eff}(\xi, r)$ rises with $r \lesssim 1.5 \text{ fm}$. At fixed energy it is a flat function of the scanning radius. At asymptotically large ξ (W), $\alpha'_{eff}(\xi, r) \rightarrow \alpha'_{\mathbf{P}} = 0.072 \text{ GeV}^{-2}$. At lower and HERA energies the subasymptotic $\alpha'_{eff}(\xi, r) \sim (0.15 - 0.20) \text{ GeV}^{-2}$ and is very close to α'_{soft} known from the Regge phenomenology of soft scattering. It means that the gBKFL dynamics predicts a substantial rise with the energy and dipole size of the diffraction slope $B(\xi, r)$ in accordance with the energy and dipole size dependence of the effective Regge slope $\alpha'_{eff}(\xi, r)$ and due to a presence of the geometrical components $\propto r^2$ in (16) and $\Delta B_d(r) \propto r^{1.7}$ in

(13) (see also (15))². The overall dipole diffraction slope contains contributions from both $B_{npt}(\xi, r)$ and $B_{pt}(\xi, r)$ and corresponding geometrical component has r^α -behaviour with $1.7 < \alpha \lesssim 2.0$. Therefore, for discussions on the qualitative level in the subsequent sections we assume (with a reasonable accuracy) an approximate r^2 -dependence of the geometrical component contribution to the dipole diffraction slope. The first direct evaluation of the dipole diffraction slope from the data on photo- and electroproduction of vector mesons is presented in [29] and is depicted in Fig. 2.

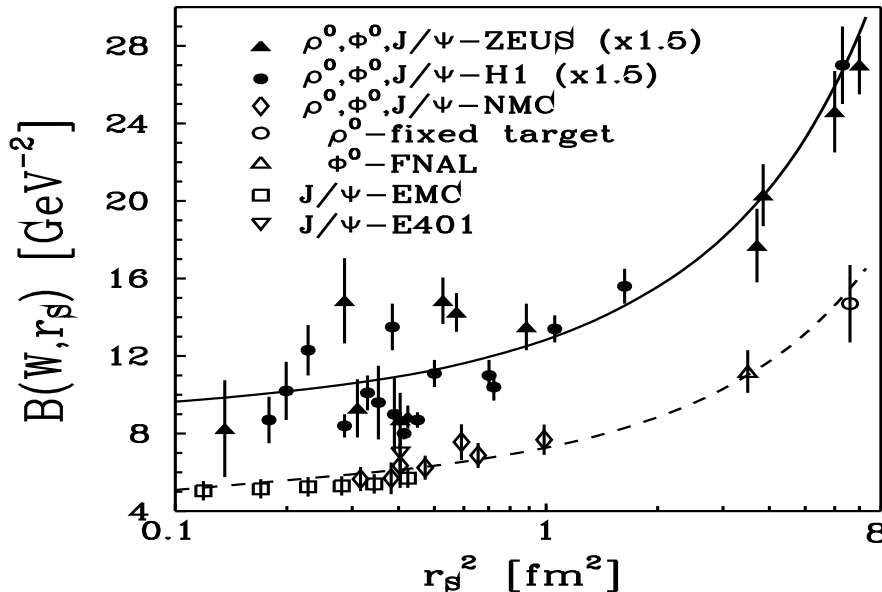


Figure 2: The dipole size dependence of the dipole cross section extracted from the data on photoproduction and electroproduction of vector mesons. The data are described in [29]. The dashed and solid curve show the dipole diffraction slope of the model [19, 16] evaluated for the c.m.s. energy $W = 15$ and 70 GeV respectively. The data points at HERA energies and the corresponding solid curve are multiplied by the factor 1.5.

3 Anomalous cross section in electroproduction of $2S$ radially excited vector mesons

The matrix element for $V'(2S)$ diffractive production contains the contributions from the region of dipole sizes above and below the node position r_n . As soon as the exact node effect encounters the Q^2 - and energy dependent cancellations from the soft (large size) and hard (small size) contributions to the $V'(2S)$ production amplitude become important. The strong Q^2 dependence of the node effect is connected with the Q^2 behaviour of the scanning radius r_S (see (2)). The energy dependence of the cancellations comes from a different energy dependence of the dipole cross section $\sigma(\xi, r)$ at different dipole sizes r .

²Dipole size behaviour of $\Delta B_d(r)$ (15) representing the geometrical contribution to the dipole diffraction slope $B_{npt}(\xi, r)$ (13) for diffractive scattering of large color dipole has the standard r^2 -dependence at small $r^2 \ll aR_N^2$ and large $r^2 \gg aR_N^2$ values of dipole size, respectively. In the intermediate region $r^2 \sim aR_N^2$, which corresponds to production of $V(1S)$ and $V'(2S)$ light vector mesons, the dipole size dependence of $\Delta B_d(r)$ can be parameterized by the power function r^α with $\alpha \sim 1.7$.

We would like to emphasize from the very beginning that the predictive power is weak and the predictions are strongly model dependent in the region of Q^2 and energy when the node effect becomes exact. Presenting and discussing in the subsequent sections the model predictions for $V'(2S)$ vector mesons we do not insist on the precise pattern of an anomalous behaviour. We present the model calculations only as an illustration of possible anomalies, which can be tested at HERA ³. We will concentrate mainly on the production of $V'(2S)$ light vector mesons because of a strong node effect and the fact that the new data obtained at HERA will be analyzed soon. In the nonrelativistic limit of heavy quarkonia, the node effect will not depend on the polarization of the virtual photon and of the produced vector meson. Not so for light vector mesons [15]. The wave functions of (T) and (L) polarized (virtual) photon are different. Different regions of z contribute to the \mathcal{M}_T and \mathcal{M}_L . Different scanning radii for production of (T) and (L) polarized vector mesons and different energy dependence of $\sigma(\xi, r)$ at these scanning radii lead to a different Q^2 and energy dependence of the node effect in production of (T) and (L) polarized $V'(2S)$ vector mesons.

There are two possible scenarios for the node effect: the undercompensation and the overcompensation regime [18]. In the undercompensation scenario, the $V'(2S)$ production amplitude $\langle V'(2S) | \sigma(\xi, r) | \gamma^* \rangle$ is dominated by the positive valued contribution coming from small dipole sizes $r \lesssim r_n$ and the $V(1S)$ and $V'(2S)$ photoproduction amplitudes have the same sign. This scenario corresponds namely to the production of $V'(2S)$ heavy vector mesons ($\Psi'(2S)$, $\Upsilon'(2S)$, ...). In the overcompensation scenario, the $V'(2S)$ production amplitude is dominated by the negative valued contribution coming from large dipole sizes $r \gtrsim r_n$, and the $V(1S)$ and $V'(2S)$ photoproduction amplitudes have the opposite sign. This scenario can correspond to the production of $V'(2S)$ light vector mesons, $\rho'(2S)$, $\omega'(2S)$ and $\phi'(2S)$ ⁴.

Let us start with (T) polarization. In the undercompensation scenario [18] a decrease of of the scanning radius with Q^2 leads to a rapid decrease of the negative contribution coming from large $r \gtrsim r_n$ and to a rapid rise of the $V'(2S)/V(1S)$ production ratio with Q^2 . The stronger the suppression of the real photoproduction of the $V'(2S)$ state, the steeper the Q^2 dependence of the $V'(2S)/V(1S)$ production ratio expected at small Q^2 . In Fig. 3 we predict the $\rho'(2S)/\rho^0$ and $\phi'(2S)/\phi^0$ (T) polarized production ratios using the wave functions from [15]. They rise by more than one order of magnitude in the range $Q^2 \lesssim 0.5 \text{ GeV}^2$. At larger $Q^2 \gtrsim 1 \text{ GeV}^2$, when the production amplitudes are dominated by dipole size $r \ll r_n$ the $V'(2S)$ and $V(1S)$ production cross sections become comparable. [18, 6].

Using the wave functions from [15] we predict the overcompensation scenario at $Q^2 = 0$ for (L) polarized $\rho'(2S)$ and $\phi'(2S)$ mesons. Consequently, the decrease with Q^2 of the scanning radius r_S leads to the *exact* cancellation of the small and large distance contributions at some value $Q_c^2 \sim 0.5 \text{ GeV}^2$ for both the $\rho'_L(2S)$ and $\phi'_L(2S)$ production. The value of Q_c^2 is slightly different for the imaginary and the real part of $V'(2S)$ production amplitude. We can not insist on the precise value of Q_c^2 which is subject to the soft-hard cancellations, our emphasis is on the likely scenario with the exact node effect at a finite Q_c^2 .

At larger Q^2 and/or smaller scanning radius one enters the above described undercompensation scenario. For both (T) and (L) polarized photons, $V'(2S)/V(1S)$ production ratios rise steeply with Q^2 on the scale $Q^2 \sim 0.5 \text{ GeV}^2$. At large Q^2 where the production of (L) polarized mesons dominates, the $\rho'(2S)/\rho^0$ and $\phi'(2S)/\phi^0$ cross section ratios level off at $\sim 0.3 - 0.4$ (see Fig. 3). This large- Q^2 limiting value of the production cross section ratios

³ Manifestations of the node effect in electroproduction on nuclei were discussed earlier, see [18] and [30]

⁴ discussion on the experimental determination of the relative sign of the $V'(2S)$ and $V(1S)$ production amplitudes using the so-called Söding-Pumplin effect [31, 32] has been already presented in [15]

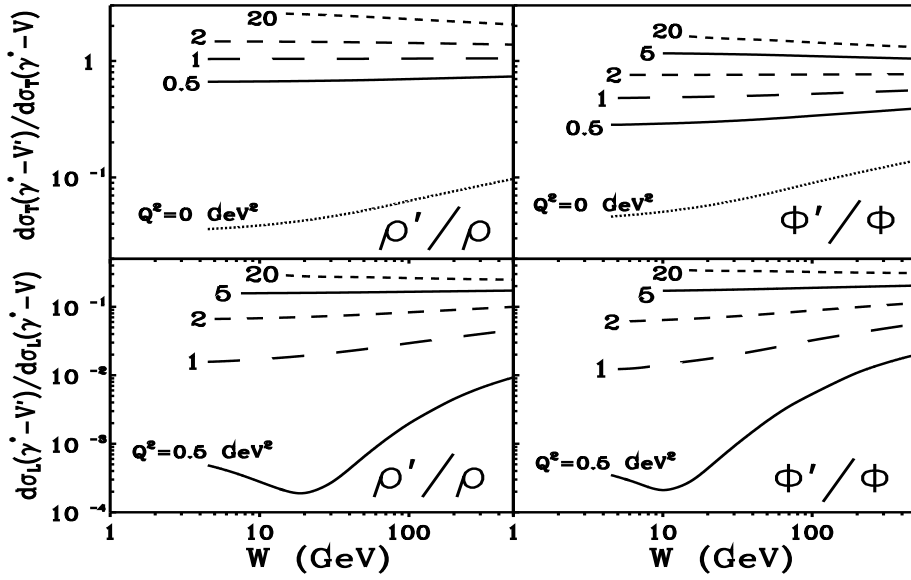


Figure 3: The color dipole model predictions for the Q^2 and W dependence of the ratios $\sigma(\gamma^* \rightarrow \rho'(2S))/\sigma(\gamma^* \rightarrow \rho^0)$ and $\sigma(\gamma^* \rightarrow \phi'(2S))/\sigma(\gamma^* \rightarrow \phi^0)$ for the (T) and (L) polarization of the vector mesons.

depends on the ratio of $V'(2S)$ and $V(1S)$ wave functions at the origin, which in potential models is subject to the detailed form of the confining potential [33].

The energy dependence of the $\rho'(2S)$ and $\phi'(2S)$ real photoproduction is shown in Fig. 4 and has again a specific pattern. In the color dipole gBFKL dynamics, the negative contribution to the $V'(2S)$ production amplitude coming from $r \gtrsim r_n$, has a slower growth with energy than the positive contribution coming from $r \lesssim r_n$. Consequently, in the undercompensation regime (which corresponds to (T) polarization) the destructive interference of these two contributions becomes weaker at higher energy and we predict a growth with energy of the $V'_T(2S)/V_T(1S)$ production cross section ratios (see Fig. 3) and (T) polarized forward production cross sections (see Fig. 4 - top boxes).

For (L) polarized $V'_L(2S)$ we have a chance of studying the Q^2 and energy dependence in the overcompensation scenario. At moderate energy and Q^2 very close to Q_c^2 but still $\lesssim Q_c^2$ the negative contribution from $r \gtrsim r_n$ still takes over in the $V'_L(2S)$ production amplitude. With increasing energy, the positive contribution to the production amplitude rises faster and gradually takes over. At some intermediate energy there is an exact cancellation of the two contributions to the production amplitude and $V'_L(2S)$ production cross section exhibits a minimum. The value of the minimum is finite because cancellations in the real and imaginary part of the production amplitude are different. Using the model wave functions from [15] we find such a nonmonotonic energy dependence of the $\rho'_L(2S)$ and $\phi'_L(2S)$ production at $Q^2 \approx 0.5 \text{ GeV}^2$, which is shown in Fig. 3 (bottom boxes) and Fig. 4 (middle boxes). At higher $Q^2 > Q_c^2$ one encounters the above described undercompensation scenario and the energy dependence of $V'_L(2S)/V_L(1S)$ production ratios and of $V'_L(2S)$ production cross sections becomes very weak.

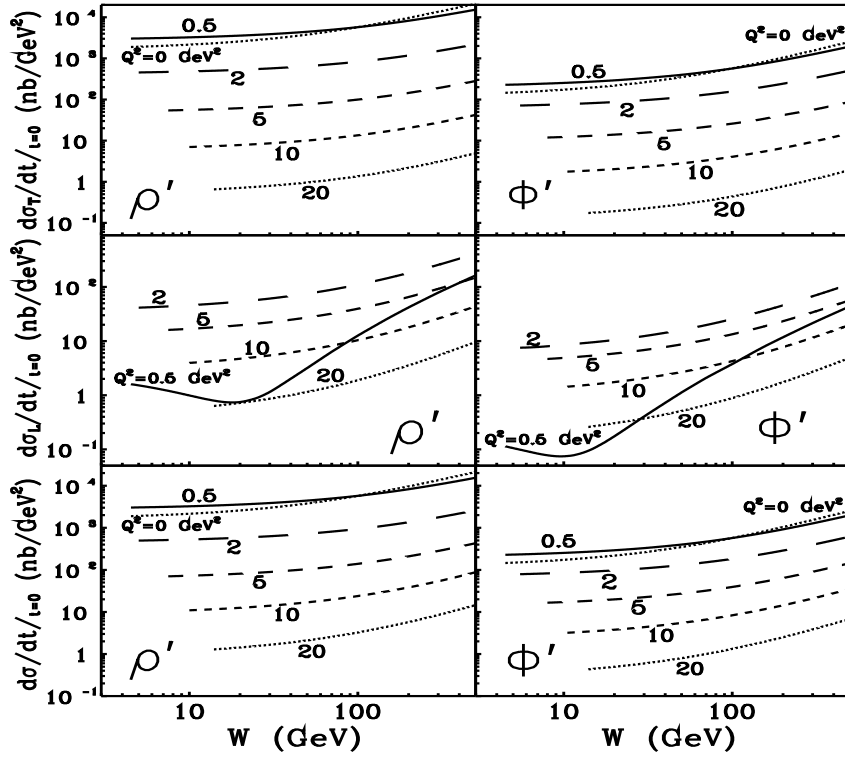


Figure 4: The color dipole model predictions of the forward differential cross sections $d\sigma_{L,T}(\gamma^* \rightarrow V')/dt|_{t=0}$ for transversely(T) (top boxes) and longitudinally (L) (middle boxes) polarized radially excited vector mesons $\rho'(2S)$ and $\phi'(2S)$ and for the polarization-unseparated $d\sigma(\gamma^* \rightarrow V')/dt|_{t=0} = d\sigma_T(\gamma^* \rightarrow V')/dt|_{t=0} + \epsilon d\sigma_L(\gamma^* \rightarrow V')/dt|_{t=0}$ for $\epsilon = 1$ (bottom boxes) as a function of the c.m.s. energy W at different values of Q^2 .

4 Anomalous diffraction slope for production of $2S$ radially excited vector mesons

For a better understanding of anomalous properties of the $V'(2S)$ diffraction slope, the generalized factorization formula (11) can be rewritten as the ratio of two matrix elements

$$B(\gamma^* \rightarrow V(V'), \xi, Q^2, \mathbf{q} = 0) = \frac{\langle V(V') | \sigma(\xi, r) B(\xi, r) | \gamma^* \rangle}{\langle V(V') | \sigma(\xi, r) | \gamma^* \rangle} = \frac{\int_0^1 dz \int d^2\mathbf{r} \sigma(\xi, r) B(\xi, r) \Psi_{V(V')}^*(\mathbf{r}, z) \Psi_{\gamma^*}(\mathbf{r}, z)}{\int_0^1 dz \int d^2\mathbf{r} \sigma(\xi, r) \Psi_{V(V')}^*(\mathbf{r}, z) \Psi_{\gamma^*}(\mathbf{r}, z)} = \frac{\mathcal{N}}{\mathcal{D}}, \quad (17)$$

where \mathcal{N} and \mathcal{D} denotes the numerator and denominator, respectively.

Anomalous properties of the diffraction slope comes namely from (17). The denominator \mathcal{D} represents the well-known production amplitude. As it was mentioned the $V(1S)$ production amplitude is dominated by contribution from dipole size $r \sim r_S$ (2). However, because of an approximate $\propto r^2$ behaviour of the slope parameter the integrand of the matrix element in the numerator \mathcal{N} of Eq. (23) is dominated by the dipole size $r = r_B \sim 5/3r_S$.

Let \mathcal{M}_+ and \mathcal{M}_- be the moduli of positive and negative valued contributions to the $V'(2S)$ production amplitude from the region of dipole sizes $r < r_n$ and $r > r_n$, and let

B_+ and B_- be the diffraction slopes for the corresponding contributions. Because of an approximate $\sim r^2$ dependence of the diffraction slope (see discussion in Sect. 2) we have a strong inequality

$$B_+ < B_- \quad (18)$$

The overall $V'(2S)$ production amplitude is $\mathcal{M}(2S) = \mathcal{M}_+ - \mathcal{M}_-$ and the corresponding overall diffraction slope for $V'(2S)$ production reads

$$\begin{aligned} B(2S) &= \frac{B_+ \mathcal{M}_+ - B_- \mathcal{M}_-}{\mathcal{M}_+ - \mathcal{M}_-} \\ &= B_+ - (B_- - B_+) \frac{\mathcal{M}_-}{\mathcal{M}_+ - \mathcal{M}_-}, \end{aligned} \quad (19)$$

which can be rewritten in a more convenient form for the following discussion

$$B(2S) - B(1S) = -(B_- - B_+) \frac{\mathcal{M}_-}{\mathcal{M}_+ - \mathcal{M}_-}, \quad (20)$$

where $B(1S) \approx B_+$ for production of $V(1S)$ vector mesons. For the diffractive production of $V'(2S)$ heavy vector mesons the production amplitude $\mathcal{M}(2S)$ is positive valued (under-compensation scenario) at $Q^2 = 0$ and consequently we predict from (20) a counterintuitive inequality $B(\Psi'(2S)) < B(J/\Psi(1S))$ [16] although the r.m.s. radius of Ψ' is much larger than $R_{J/\Psi}$. However, we will manifest below that this is not always true in production of $V'(2S)$ light vector mesons.

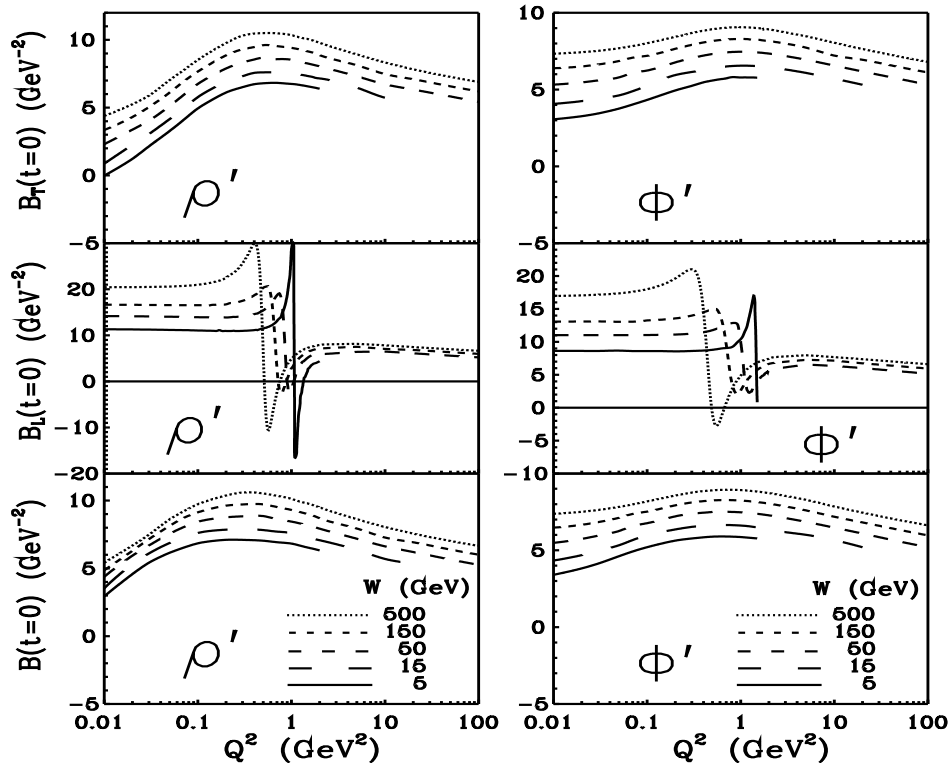


Figure 5: - The color dipole model predictions for the Q^2 dependence of the diffraction slope $B(t = 0)$ for production of transversely (T) (top boxes), longitudinally (L) (middle boxes) polarized and polarization-unseparated (T) + ϵ (L) (bottom boxes) $\rho'(2S)$ and $\phi'(2S)$ for $\epsilon = 1$ at different values of the c.m.s. energy W .

Undercompensation scenario

The undercompensation scenario ($\mathcal{D} > 0$ in (17)) corresponds to the production of (T) polarized $\rho'(2S)$ and $\phi'(2S)$ at $Q^2 = 0$ using the wave functions from Ref. [15]. Because of $r_B > r_S$, there are two possibilities concerning the sign of \mathcal{N} in Eq. (17).

i.) $\mathcal{N} < 0$; \mathcal{N} and \mathcal{D} have the opposite sign. Consequently, the diffraction slope in the photoproduction limit is negative valued. This pattern corresponds to diffractive photoproduction of $\rho'_T(2S)$ at small energy (see Figs. 5 and 6 - top boxes).

ii.) $\mathcal{N} > 0$; \mathcal{N} and \mathcal{D} have the same sign. Consequently, the diffraction slope in the photoproduction limit is positive valued. This pattern corresponds to diffractive photoproduction of $\phi'_T(2S)$ (see Figs. 5 and 6 - top boxes) and the node effect is weaker in comparison with $\rho'_T(2S)$ photoproduction.

In both cases we predict from Eq. (20) the counterintuitive inequalities $B(\rho'_T(2S)) < B(\rho_T(1S))$ and $B(\phi'_T(2S)) < B(\phi_T(1S))$, which are analogical to that for charmonium diffractive photoproduction [16].

A decrease of the scanning radius with Q^2 leads to a very rapid decrease of the negative valued contribution to the diffraction slope coming from $r \gtrsim r_n$ and consequently leads to a steep rise of $B(V'_T(2S))$ with Q^2 . The higher is Q^2 the weaker is the node effect and the smaller is the difference $|B(2S) - B(1S)|$. At still larger Q^2 and at fixed energy W the slope parameter $B(V'_T(2S))$ exhibits a broad maximum at some value of $Q^2_T \in (0.5 - 2.0) \text{ GeV}^2$. At very large $Q^2 \gg m_V^2$ when the node effect becomes negligible, $B(2S) \sim B(1S)$ and $B(V'_T(2S))$ decreases monotonously with Q^2 following the Q^2 dependence of $B(V_{L,T}(1S))$. The above described pattern of nonmonotonic Q^2 dependence of the diffraction slope is depicted in Fig. 5 (bottom boxes) for both the $\rho'_T(2S)$ and $\phi'_T(2S)$ production.

Overcompensation scenario

The overcompensation scenario ($\mathcal{D} < 0$ in (17)), corresponds to the production of (L) polarized $\rho'(2S)$ and $\phi'(2S)$ at $Q^2 = 0$ using the wave functions from Ref. [15]. Because of $r_B > r_S$, $\mathcal{N} < 0$ and has the same sign as \mathcal{D} . Consequently, the diffraction slope in the photoproduction limit is positive valued as it can be expected also from the undercompensation regime described above. The sign of the diffraction slope $B(2S)$ at $Q^2 = 0$ can not distinguish between the overcompensation and undercompensation scenarios. However, because of $\mathcal{M}(2S) < 0$ the difference $B(2S) - B(1S)$ is positive valued (see Eq. (20)). As the result we predict the expected inequalities $B(\rho_L(1S)) < B(\rho'_L(2S))$ and $B(\phi_L(1S)) < B(\phi'_L(2S))$, what is a new result in comparison with the color dipole predictions for heavy vector mesons presented in the paper [16].

With the decrease of the scanning radius with Q^2 there is a rapid decrease of the negative contributions to \mathcal{N} and \mathcal{D} coming from $r \gtrsim r_n$. For some $Q^2 \sim Q_L^2 \in (0.5 - 1.5) \text{ GeV}^2$ one encounters the exact node effect firstly for the denominator \mathcal{D} and $B(V'_L(2S))$ has a peak for both the $\rho'_L(2S)$ and $\phi'_L(2S)$ production. The value of $B(V'_L(2S))$ corresponding to this exact node effect will be finite due to a different node effect for the real and imaginary part of the production amplitude. The onset of the node effect causes also the rapid continuous transition of $B(V'_L(2S))$ from positive to negative values when the matrix element \mathcal{D} passes from the overcompensation to undercompensation regime. Consequently, for $Q^2 > Q_L^2$, $\mathcal{D} > 0$, \mathcal{N} is kept to be negative valued and $B(V'_L(2S))$ starts to rise from its minimal negative value (see Fig. 5 - middle boxes). At still larger Q^2 the following pattern of the Q^2 behaviour of $B(V'_L(2S))$ is analogical to that for Q^2 dependence of $B(V'_T(2S))$. For the production of polarization unseparated $V'(2S)$, the anomalous properties of $B(V'_L(2S))$ are essentially invisible and the corresponding slope parameter $B(V'(2S))$ has an analogical Q^2

dependence as $B(V'_T(2S))$ and is shown in Fig. 5 (bottom boxes). Here we can not insist on the precise value of Q_L^2 which is again a subject of the soft-hard cancellations. We would like only to emphasize that the exact node effect for $B(V'_L(2S))$ is at a finite Q_L^2 .

To conclude the Q^2 dependence of $B(2S)$, the undercompensation scenario is characterized by a broad maximum at $Q^2 \sim Q_T^2$ and can be tested experimentally at HERA measuring the virtual photoproduction of the $\rho'(2S)$ and $\phi'(2S)$ at $Q^2 \in (0 - 10)$ GeV² and at different values of energy. However, the overcompensation scenario is characterized by a sharp peak followed by a very rapid transition of the diffraction slope from positive to negative values at $Q^2 \sim Q_L^2$ and then by a broad maximum at $Q^2 \sim Q_L^2$ and can be also investigated at HERA separating (L) polarized $\rho'_L(2S)$ and $\phi'_L(2S)$ at moderate $Q^2 \in (0.1 - 5.0)$ GeV².

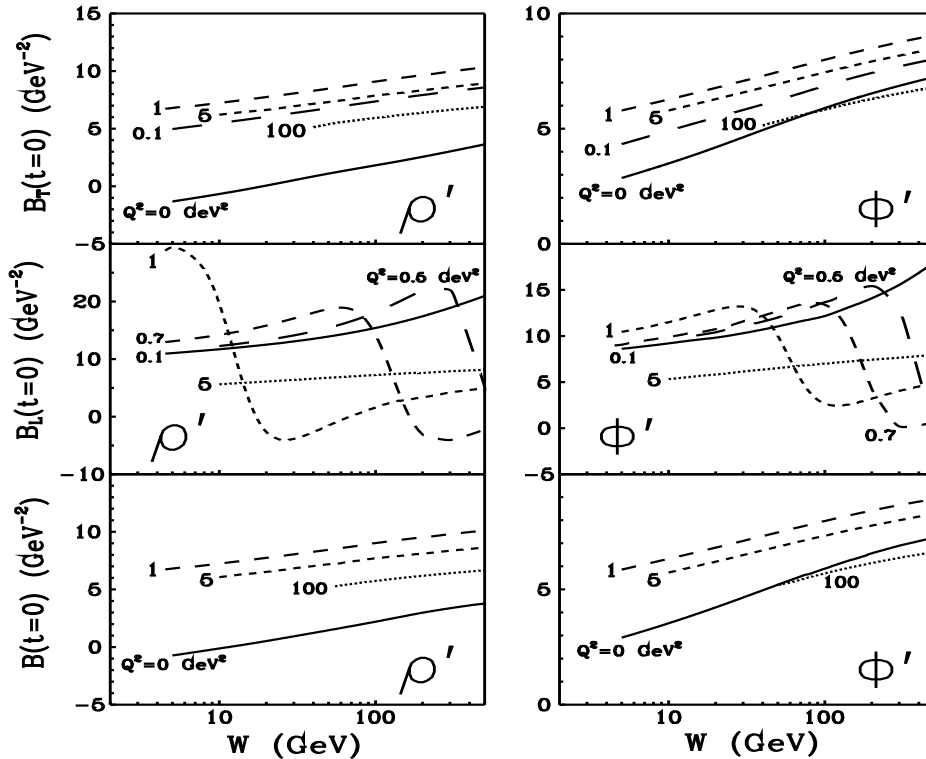


Figure 6: - The color dipole model predictions for the W dependence of the diffraction slope $B(t = 0)$ for production of transversely (T) (top boxes), longitudinally (L) (middle boxes) polarized and polarization-unseparated (T) + ϵ (L) (bottom boxes) $\rho'(2S)$ and $\phi'(2S)$ for $\epsilon = 1$ at different values of Q^2 .

The energy dependence of $B(V'(2S))$ at different Q^2 is shown in Fig. 6 and has its own peculiarities. Let us start with $B(V'_T(2S))$ at $Q^2 = 0$ when the production amplitude is in the undercompensation regime, $\mathcal{D} > 0$. Fig. 6 demonstrates (top boxes) steeper rise with energy of the diffraction slope at lower Q^2 and confirms the expectation coming from the gBFKL dynamics that the energy dependence of $B'_T(2S)$ is given mainly by the effective Regge slope α' (see Eqn. (13) and (16), which decreases with Q^2 .

The successful separation of (L) polarized $V'_L(2S)$ mesons at HERA offers an unique possibility to study an anomalous energy dependence of the diffraction slope in the overcompensation scenario. At $Q^2 = 0$ both the \mathcal{N} and \mathcal{D} of Eq. (17) are negative valued. At moderate energy and Q^2 close but smaller than Q_L^2 , the negative valued contribution coming from $r \gtrsim r_n$ still takes over in \mathcal{D} ($\mathcal{N} < 0$ as well due to $r_B > r_S$). Because of a steeper rise

with energy of the positive contribution to the $V'(2S)$ production amplitude coming from $r \lesssim r_n$ than the negative contribution coming from $r \gtrsim r_n$, we find an exact cancellation of these two contributions to \mathcal{D} and a maximum of the diffraction slope $B(V'_L(2S))$ at some intermediate energy followed by its rapid continuous transition from the positive to negative values, when \mathcal{D} passes from the overcompensation to the undercompensation regime. Different node effect for the real and imaginary part of the production amplitude provides such a continuous transition. At larger energies $\mathcal{D} > 0$ (undercompensation regime) and consequently $B(V'_L(2S))$ is negative valued and starts to rise from its minimal negative value. Such a situation is depicted in Fig. 6 (middle boxes), where we predict with the wave functions from Ref. [15] such a nonmonotonic energy behaviour of $B(V'_L(2S))$ for both $\rho'(2S)$ and $\phi'(2S)$ production at $Q^2 \lesssim Q_L^2 \in (0.5 - 1.5)$ GeV². The position of the maximum W_t and the transition from the positive to negative values of $B(V'_L(2S))$ depends on Q^2 and can be measured at HERA. At higher Q^2 and smaller scanning radii, the further pattern of the energy behaviour for $B(V'_L(2S))$ is analogical to that for $B(V'_T(2S))$.

If (T) and (L) polarized $V'_T(2S)$ and $V'_L(2S)$ mesons will be separated experimentally there is a chance for experimental determination of a concrete scenario in (T) and (L) polarized $V'(2S)$ production amplitude. The simplest test can be realized in the photoproduction limit ($Q^2 = 0$) for a broad energy range. If the data will report the counterintuitive inequality $B(2S) < B(1S)$ ($B(2S)$ can be also negative valued) then $V'(2S)$ production amplitude is in the undercompensation regime (positive valued). In the opposite case when the expected inequality $B(2S) > B(1S)$ will be obtained from the data then $V'(2S)$ production amplitude is in the overcompensation regime (negative valued). For the production of (L) polarized vector mesons the values of Q^2 should be high enough to have the data with a reasonable statistics however, must not be very large in order to have a considerably strong node effect. We propose the range of $Q^2 \in (0.5 - 5.0)$ GeV² for exploratory study of the overcompensation scenario at HERA.

5 Anomalous t dependence of the differential cross section for production of $2S$ radially excited vector mesons

We discuss now the possible peculiarities in t dependent differential cross section $d\sigma/dt$ for $V'(2S)$ production. We would like to emphasize again that we do not insist on the precise form of the t dependence of $d\sigma/dt$, the main emphasis is on the likely pattern of the t dependence coming from the node effect. The differential cross section is calculated using the expressions (5) and (6) for (T) and (L) production amplitudes in conjunction with Eqs. (8), (9), (13) and (16). Because of an approximate $\propto r^2$ behaviour of the geometrical contribution to the diffraction slope (see discussion in Sect. 2), the large size negative contribution to the production amplitude from the region $r > r_n$ corresponds to larger value of the diffraction slope than the small size contribution from the region $r < r_n$. It means that the negative contribution to the $V'(2S)$ production amplitude has a steeper t dependence than the positive contribution. Let t -dependent production amplitude be

$$\mathcal{M}(t) = c_+ \exp(-\frac{1}{2}B_+t) - c_- \exp(-\frac{1}{2}B_-t), \quad (21)$$

where c_+ and c_- are the contributions to the amplitude from the region below and above the node position with the corresponding effective diffraction slopes B_+ and B_- , respectively

($B_+ < B_-$). Inequality $c_+ > c_-$ means the undercompensation whereas $c_+ < c_-$ the overcompensation regime. The destructive interference of these two contributions results in a decrease of the effective diffraction slope for $V'(2S)$ meson production towards small t in contrary to the familiar increase for the $V(1S)$ meson production. Such a situation is shown in Fig. 7, where we present the model predictions for the differential cross section $d\sigma(\gamma^* \rightarrow V(V'))/dt$ for production of $V(1S)$ and $V'(2S)$ mesons at different c.m.s. energies W and at $Q^2 = 0$.

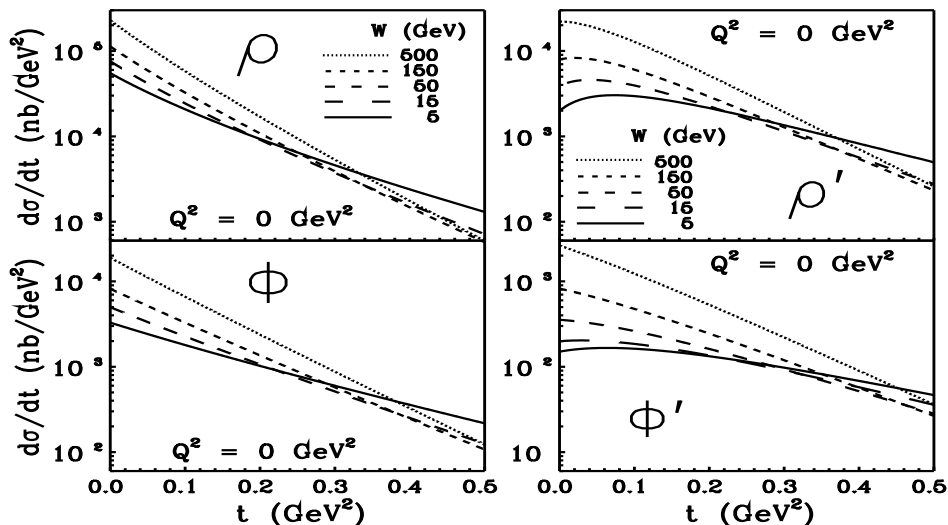


Figure 7: - The color dipole model predictions for the differential cross sections $d\sigma(\gamma^* \rightarrow V(V'))/dt$ for the real photoproduction ($Q^2 = 0$) of the $\rho^0, \rho'(2S), \phi^0$ and $\phi'(2S)$ at different values of the c.m.s. energy W .

Real photoproduction measures the purely transverse cross section. As was already mentioned, $V'(2S)$ production amplitude is in undercompensation regime ($\mathcal{D} > 0$). However, because of $r_B > r_S$, the numerator $\mathcal{N} < 0$ at $W \lesssim 150$ GeV for $\rho'(2S)$ production and at $W \lesssim 30$ GeV for $\phi'(2S)$ production. As the result, the diffraction slope is negative valued at $Q^2 = 0$. At $t > 0$ the node effect becomes weaker. The higher is t the weaker is the node effect as a consequence of the destructive interference (21) described above. Consequently, $d\sigma(\gamma^* \rightarrow V'(2S))/dt$ firstly rises with t , flattens off at $t \in (0.0 - 0.2)$ GeV² having a broad maximum. At large t , the node effect is weak and $d\sigma(\gamma^* \rightarrow V'(2S))/dt$ decreases with t monotonously as for $V(1S)$ production. The position of the maximum can be roughly evaluated from (21)

$$t_{max} \sim \frac{1}{2(B_- - B_+)} \log \left[\frac{c_-^2 B_-^2}{c_+^2 B_+^2} \right], \quad (22)$$

with the supplementary condition

$$\frac{c_-}{c_+} > \frac{B_+}{B_-} \quad (23)$$

If the condition (23) is not fulfilled $d\sigma(\gamma^* \rightarrow V'(2S))/dt$ has no maximum and exhibits a standard monotonous t -behaviour. The predicted nonmonotonic t -behaviour of $d\sigma/dt$ for $\rho'(2S)$ and $\phi'(2S)$ production in the photoproduction limit is strikingly different especially at smaller energies from the familiar decrease with t of $d\sigma(\gamma \rightarrow \rho^0(1S))/dt$ and $d\sigma(\gamma \rightarrow \phi^0(1S))/dt$ (see Fig. 7).

At larger energies, $W \gtrsim 150$ GeV for the $\rho'(2S)$ photoproduction and $W \gtrsim 30$ GeV for $\phi'(2S)$ photoproduction, the node effect becomes weaker the diffraction slope is positive

valued (both $\mathcal{N} > 0$ and $\mathcal{D} > 0$) and the nonmonotonic t dependence of the differential cross section is changed for the monotonic one but still the effective diffraction slope decreases slightly towards small t (see Fig. 7).

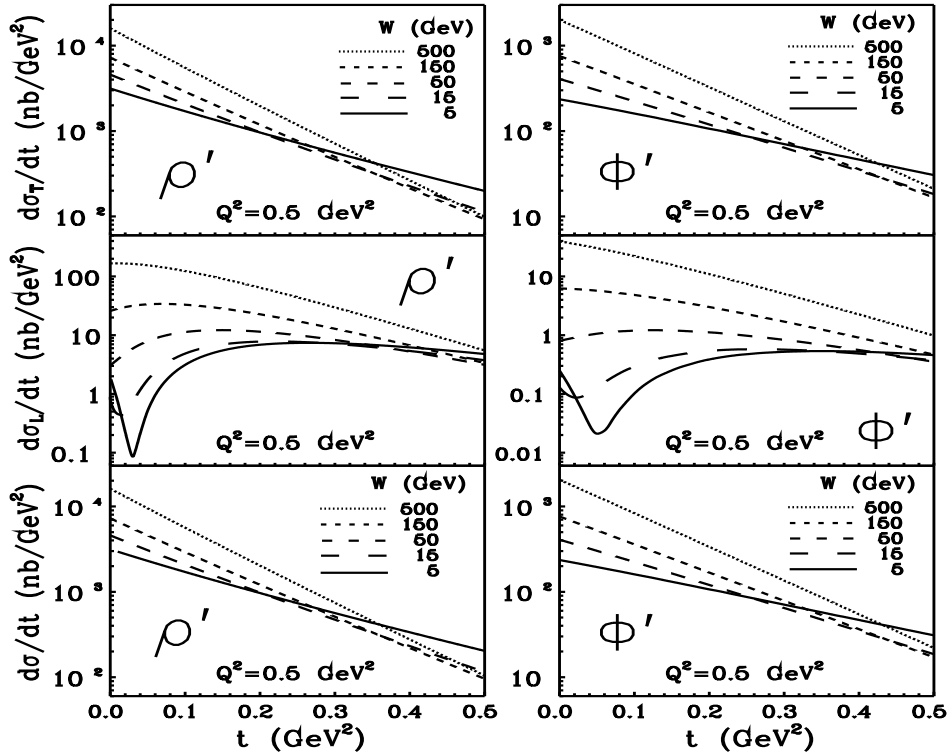


Figure 8: - The color dipole model predictions for the differential cross sections $d\sigma_{L,T}(\gamma^* \rightarrow V'(2S))/dt$ for transversely (T) (top boxes) and longitudinally (L) (middle boxes) polarized radially excited $\rho'(2S)$, $\phi'(2S)$ and for the polarization-unseparated $d\sigma(\gamma^* \rightarrow V')/dt = d\sigma_T(\gamma^* \rightarrow V'(2S))/dt + \epsilon d\sigma_L(\gamma^* \rightarrow V'(2S))/dt$ for $\epsilon = 1$ (bottom boxes) at $Q^2 = 0.5 \text{ GeV}^2$ and different values of the c.m.s. energy W .

Because of a possible overcompensation scenario for $\rho'_L(2S)$ and $\phi'_L(2S)$ mesons at small Q^2 (see also previous sections), we present in Fig. 8 the model predictions for $d\sigma(\gamma^* \rightarrow V'(2S))/dt$ at different energies W and at fixed $Q^2 = 0.5 \text{ GeV}^2$ for the production of (T), (L) polarized and polarization unseparated $\rho'(2S)$ and $\phi'(2S)$ mesons. As it was mentioned above, at $Q^2 = 0.5 \text{ GeV}^2$ the production amplitude for $\rho'_L(2S)$ and $\phi'_L(2S)$ mesons is still in overcompensation regime $\mathcal{D} < 0$ ($\mathcal{N} < 0$ as well) and the corresponding diffraction slope $B(V'_L(2S))$ is positive valued at small energies $W \lesssim 20 \text{ GeV}$. It results in a very spectacular pattern of anomalous t dependence for $d\sigma(\gamma^* \rightarrow V'_L(2S))/dt$ shown in Fig. 8 (middle boxes). With rising t due to above described destructive interference of two contributions to the production amplitude (see (21)), one encounters the exact node effect at some $t \sim t_{min}$. Consequently, $d\sigma/dt$ firstly falls down rapidly with t having a minimum at $t \sim t_{min}$. At still larger t when the overcompensation scenario of t -dependent production amplitude is changed for the undercompensation one and the slope parameter becomes to be negative valued, $d\sigma(\gamma^* \rightarrow V'_L(2S))/dt$ starts to rise with t and further pattern of t -behaviour is analogical to that for $V'_T(2S)$ production (see Fig. 7).

The position of the minimum t_{min} is model dependent and can be roughly estimated

from (21)

$$t_{min} \sim \frac{1}{2(B_- - B_+)} \log \left[\frac{c_-^2}{c_+^2} \right]. \quad (24)$$

The gBFKL model predictions give $t_{min} \sim 0.03 \text{ GeV}^2$ for $\rho'_L(2S)$ production and $t_{min} \sim 0.05 \text{ GeV}^2$ for $\phi'_L(2S)$ production at $Q^2 = 0.5 \text{ GeV}^2$ and at $W = 5 \text{ GeV}$. However, we can not exclude a possibility that this minimum will take a place at other values of t . At $Q^2 < 0.5 \text{ GeV}^2$, t_{min} will be located at larger values of t . At higher energy, the position of t_{min} is shifted to a smaller value of t unless the exact node effect is reached at $t = 0$. At still larger energy, when the $V'_L(2S)$ production amplitude is in undercompensation regime, this minimum disappears and we predict the pattern of t -behaviour for $d\sigma(\gamma^* \rightarrow V'_L(2S))/dt$ analogical to that for $d\sigma(\gamma \rightarrow V'_T(2S))/dt$ in the photoproduction limit depicted in Fig. 7. These predicted anomalies can be tested at HERA measuring the diffractive electroproduction of $V'(2S)$ light vector mesons in separate polarizations (T) and (L).

6 Conclusions

We study the diffractive photo- and electroproduction of radially excited $V'(2S)$ vector mesons within the color dipole gBFKL dynamics. We present a short review of possible anomalies, which can be presently observed at HERA experiments. The predicted anomalies are connected with the node position in $V'(2S)$ radial wave function.

Firstly, we present a rich pattern of anomalous Q^2 and energy dependence of the production cross section. As a consequence of the node effect especially for light vector mesons ($\rho'(2S), \phi'(2S)$) we predict a very strong suppression of the $V'(2S)/V(1S)$ production ratio in the real photoproduction limit of very small Q^2 . For the longitudinally polarized $V'(2S)$ mesons we find a plausible overcompensation scenario leading to a sharp dip of the longitudinal cross section $\sigma_L(2S)$ at some finite $Q^2 = Q_c^2 \sim 0.5 \text{ GeV}^2$. The position Q_c^2 of this dip depends on the energy and leads to a nonmonotonic energy dependence of $\sigma_L(2S)$ at fixed Q^2 . At larger Q^2 and smaller scanning radius we predict a steep rise of the $V'(2S)/V(1S)$ cross section ratio. The flattening of this $2S/1S$ ratio at large Q^2 is a non-negotiable prediction from the color dipole dynamics.

Further predictions are related to the anomalous pattern of Q^2 and energy behaviour of the diffraction slope for the production of $V'(2S)$ vector mesons. At moderate energies, we find a nonmonotonic Q^2 dependence of the slope parameter which can be tested at HERA in the range of $Q^2 \in (0 - 10) \text{ GeV}^2$. For the production of (L) polarized $V'(2S)$ as a consequence of the overcompensation scenario we find a sharp peak followed immediately by a very rapid transition of the slope parameter from positive to negative values at $Q^2 \sim Q_L^2 \in (0.5 - 1.5) \text{ GeV}^2$. The position of this rapid transition Q_L^2 is energy dependent and leads to a nonmonotonic energy dependence of $B(V'_L(2S))$ at fixed Q^2 . At $Q^2 = 0$ when the node effect is strong, for the undercompensation scenario we predict a counterintuitive inequality $B(V'(2S)) < B(V(1S))$. However, for overcompensation scenario we predict the expected standard inequality $B(V'(2S)) > B(V(1S))$. This is a very crucial point of a possible experimental determination of a concrete scenario extracting from the data at HERA the $B(V'(2S))$ diffraction slope in the photoproduction limit.

The last class of predictions concerns to an anomalous t dependence of the $V'(2S)$ differential cross section. The origin is in destructive interference of the large distance negative contribution to the production amplitude from the region above the node position with a steeper t -dependence and the small distance positive contribution to the production amplitude from the region below the node position with a weaker t -dependence. As the

result, we predict at $Q^2 = 0$ a nonmonotonic t dependence of $d\sigma(\gamma \rightarrow V'_T(2S))/dt$ and a decreasing diffraction slope for $V'_T(2S)$ mesons towards small values of t in contrary with the familiar increase of $B(V(1S))$ for $V(1S)$ vector mesons. The differential cross section firstly rises with t having a broad maximum. At larger t when the node effect is still weaker, $d\sigma(\gamma \rightarrow V'_T(2S))/dt$ has the standard monotonic t -behaviour as for production of $V(1S)$ vector mesons. For production of (L) polarized $V'_L(2S)$ mesons, there is overcompensation at $t = 0$ leading to a dip (minimum) of the differential cross section at $t \sim t_{min}$. The position of t_{min} is energy dependent and is the result of the model dependent soft-hard cancellations.

To conclude, if the data will exhibit a dip (minimum) in energy (Q^2) dependence of the $V'(2S)$ production cross section, $V'(2S)/V(1S)$ cross section ratio, diffraction slope and in t dependence of the differential cross section $d\sigma/dt$ then the corresponding $V'(2S)$ production amplitude is in the overcompensation regime. Otherwise the $V'(2S)$ production amplitude is in the undercompensation regime.

References

- [1] A.Donnachie and P.V.Landshoff, *Phys. Lett.* **B185** (1987) 403;
J.R.Cuddell, *Nucl. Phys.* **B336** (1990) 1.
- [2] B.Z.Kopeliovich and B.G.Zakharov, *Phys. Rev.* **D44** (1991) 3466.
- [3] M.G.Ryskin, *Z. Phys.* **C57** (1993) 89.
- [4] B.Z.Kopeliovich, J.Nemchik, N.N.Nikolaev and B.G.Zakharov, *Phys. Lett.* **B309** (1993) 179.
- [5] B.Z.Kopeliovich, J.Nemchik, N.N.Nikolaev and B.G.Zakharov, *Phys. Lett.* **B324** (1994) 469.
- [6] J.Nemchik, N.N.Nikolaev and B.G.Zakharov, *Phys. Lett.* **B341** (1994) 228.
- [7] S.J.Brodsky et al., *Phys. Rev.* **D50** (1994) 3134.
- [8] J.R.Forshaw and M.G.Ryskin, *Z. Phys.* **C** (1995) to be published.
- [9] E.Gotsman, E.M.Levin and U.Maor, *Nucl. Phys.* **B464** (1996) 251.
- [10] E.A.Kuraev, L.N.Lipatov and S.V.Fadin, *Sov. Phys. JETP* **44** (1976) 443; **45** (1977) 199.
- [11] Yu.Yu.Balitsky and L.N.Lipatov, *Sov. J. Nucl. Phys.* **28** (1978) 822.
- [12] L.N.Lipatov, *Sov. Phys. JETP* **63** (1986) 904;
L.N.Lipatov, in: *Perturbative Quantum Chromodynamics*, ed. by A.H.Mueller, World Scientific (1989).
- [13] N.Nikolaev and B.G.Zakharov, *JETP* **78** (1994) 598; *Z. Phys.* **C64** (1994) 631.
- [14] N.N.Nikolaev, B.G.Zakharov and V.R.Zoller, *JETP Letters* **59** (1994) 6; *JETP* **78** (1994) 866; *Phys. Lett.* **B328** (1994) 486.
- [15] J.Nemchik, N.N.Nikolaev, E.Predazzi and B.G.Zakharov, *Z. Phys* **C75** (1997) 71.

- [16] J.Nemchik, N.N.Nikolaev, E.Predazzi, B.G.Zakharov and V.R.Zoller, *JETP* **86** (1998) 1054.
- [17] N.N.Nikolaev, *Comments on Nucl. Part. Phys.* **21** (1992) 41.
- [18] J.Nemchik, N.N.Nikolaev and B.G.Zakharov, *Phys. Lett.* **B339** (1994) 194.
- [19] N.N.Nikolaev, B.G.Zakharov and V.R.Zoller, *Phys. Lett.* **B366** (1996) 337
- [20] N.N.Nikolaev, B.G.Zakharov and V.R.Zoller, *JETP Lett.* **60** (1994) 694.
- [21] J.Nemchik, *Anomalous t -dependence in diffractive electroproduction of $2S$ radially excited light vector mesons at HERA hep-ph-0003244*, submitted to *Eur. J. Phys. C*
- [22] J.Nemchik, *The wave function of $2S$ radially excited vector mesons from data for diffraction slope hep-ph-0003245*, submitted to *Phys. Rev. D*
- [23] J.B.Kogut and D.E.Soper, *Phys. Rev.* **D1** (1970) 2901.
- [24] N.N. Nikolaev and B.G. Zakharov, *Z. Phys.* **C49** (1991) 607; *Z. Phys.* **C53** (1992) 331.
- [25] V.N.Gribov and A.A.Migdal, *Sov. J. Nucl. Phys.* **8** (1969) 703.
- [26] N.N.Nikolaev and B.G.Zakharov, *Phys. Lett.* **B327** (1994) 149.
- [27] J.Nemchik, N.N.Nikolaev, E.Predazzi and B.G.Zakharov, *Phys. Lett.* **B374** (1996) 199.
- [28] A.Schiz et al., *Phys. Rev.* **D24** (1981) 26.
J.P.Burq et al., *Phys. Lett.* **B109** (1982) 111.
- [29] J.Nemchik, *Color dipole systematics of the diffraction slope in diffractive photo- and electroproduction of vector mesons hep-ph-0008161* (2000), submitted to *Phys. Lett. B*
- [30] O.Benhar, B.G.Zakharov, N.N.Nikolaev et al., *Phys. Rev. Lett.* **74** (1995) 3565;
O.Benhar, S.Fantoni, N.N.Nikolaev et al., *Zh. Exp. Teor. Fiz.* **111** (1997) 769.
- [31] P.Söding, *Phys. Lett.* **19** (1966) 702.
- [32] J.Pumplin, *Phys. Rev.* **D2** (1970) 1859.
- [33] W.Buchmüller, S.-H.H.Tye, *Phys. Rev.* **D24** (1981) 132.